Resolving gas-phase metallicity in galaxies

Carton, D.J.

5

A dependency between the mass-metallicity relation and the metallicity gradients of galaxies

The relationship between a galaxy's stellar mass and its gas-phase metallicity results from the complex interplay between star formation and the inflow and outflow of gas. Since the gradient of metals in galaxies is also influenced by the same processes, it is therefore natural to contrast the metallicity gradient with the mass–metallicity relation. Here we study the interrelation of the stellar mass, central metallicity and metallicity gradient, using a sample of 72 galaxies spanning $0.13 < z < 0.84$ with reliable metallicity gradient estimates. We find that typically the galaxies that fall below the mean mass–metallicity relation have flat or inverted metallicity gradients. We quantify their relationship taking full account of the covariance between the different variables and find that at fixed mass the central metallicity is anti-correlated with the metallicity gradient. We argue that this is consistent with a scenario that suppresses the central metallicity either through the inflow of metal poor gas or outflow of metal enriched gas.

David Carton, Jarle Brinchmann

1 Introduction

The existence of a correlation between the metallicity[1] and luminosity in galaxies has been known for a long time (Lequeux et al. 1979; Skillman et al. 1989), while more recently it has been argued that a more fundamental relation is between metallicity and galaxy mass (Garnett 2002; Tremonti et al. 2004; Foster et al. 2012). The existence of such a relationship is not particularly surprising from a theoretical point of view, with a variety of models predicting a correlation, e.g. leaky box models (Tremonti et al. 2004; Finlator & Davé 2008) and bathtub models (Bouché et al. 2010; Davé et al. 2012; Lilly et al. 2013).

Reducing the relationship between stellar mass and metallicity to a one-dimensional one is, however, over-simplified; there is significant scatter in the relationship and this scatter contains important physical information. As a result there have been a number of studies over the last decade trying to understand what physical properties cause the scatter. These include specific star-formation rates and sizes (e.g. Ellison et al. 2008), the star-formation rate (e.g. Lara-López et al. 2010; Mannucci et al. 2010) and gas content (e.g. Bothwell et al. 2013) to mention a few. There has been particular interest in identifying whether these relations are universal (redshift independent) and which of them is the most fundamental.

Chemical evolution models can be helpful for interpreting physics underlying these relations. For instance, the bathtub models typically assume the star-formation rate (SFR) in a galaxy is set by either the total amount of gas in the system, or the net rate at which gas in accreted to the system. In these models it is therefore the balance of inflows and outflows that governs the mass–metallicity relations.

But, to really grasp the nature of these inflow and outflow processes it is desirable to have spatially resolved the metallicity in galaxies. In other words, do the galaxies that fall below the bulk of galaxies on the mass–metallicity relation have spuriously low metallicities throughout their discs, or is the low metallicity gas concentrated in the central regions?

In this work we will study the mass – central metallicity relation for a modest sample of intermediate redshift galaxies ($0.1 \lesssim z \lesssim 0.8$). We will also explore whether there is an additional dependency between central metallicity and the metallicity gradient of these galaxies.

In Section 2 we outline the data used. In Section 3 we explore dependencies of central metallicity on both mass and metallicity gradient. Finally we comment on and summarize our findings in Sections 4 & 5, respectively.

Throughout the paper we assume a ΛCDM cosmology with $H_0 = 70\ \mathrm{km\,s^{-1}\,Mpc^{-1}}$, $\Omega_\mathrm{m} = 0.3$ and $\Omega_\Lambda = 0.7$.

2 Data

The galaxy sample and data that we use here were presented in Carton et al. (in prep.; herein Chapter 4). Therein we measured the metallicity profile for 94 galaxies observed with the Multi Unit Spectroscopic Explorer (MUSE; Bacon et al. (2010, and in prep.)). In this previous work we focused exclusively on the metallicity gradients in these galaxies, however, here we will also discuss the central metallicities of these galaxies.

In this paper we will only consider the 72 galaxies that were found to have reliable metallicity gradients in Chapter 4. These galaxies span a range of redshifts between $0.13 < z < 0.84$. We derive central metallicities, $\log_{10} Z_0$, and metallicity gradients, $\nabla_r (\log_{10} Z)$, using nebular emission-lines observed with MUSE. By applying a forward-modelling technique

[1] Throughout this work, unless otherwise noted, the gas-phase abundance of oxygen ($12 + \log_{10}(\mathrm{O/H})$) will simply be referred to as metallicity.

presented in Carton et al. (2017) we are able to correct for the resolution loss caused by atmospheric seeing. The stellar masses, $\log_{10} M_*$, of the galaxies are estimated from multi-band photometry, using FAST (Kriek et al. 2009).

In the model the metallicity is taken to be a linear function of the distance from the centre of the galaxy. The metallicity gradient is the slope of this function and the central metallicity the intercept at $r = 0$. As a result we expect these quantities to be anti-correlated, e.g. galaxies with steep negative metallicity gradients will have higher central metallicities. The degree to which $\log_{10} Z_0$ and $\nabla_r (\log_{10} Z)$ are correlated depends on both the spatial resolution and the signal-to-noise (S/N) of the data, and thus varies from galaxy to galaxy.

There is another reason why these two parameters are correlated. For galaxies above $z \gtrsim 0.4$, our metallicities are primarily constrained by the line ratios of [O II]3726,3729, Hβ and [O III]5007. It is well known that metallicities defined from only these lines suffer from degeneracy between the metallicity and ionization-parameter (see Kewley & Dopita 2002). In our modelling we make the empirically motivated assumption that the ionization-parameter and metallicity are anti-correlated within a galaxy. Doing so mitigates against this degeneracy, but induces additional covariance between the central metallicity and the metallicity gradient of the galaxy.

Nevertheless, because our forward-modelling technique provides a joint posterior probability distribution of $\log_{10} Z_0$ and $\nabla_r (\log_{10} Z)$, we are able to quantify the effects of both this and the slope/intercept degeneracy. For simplicity (and numerical stability/convergence) we approximate the joint posterior as a 2D normal distribution. Similarly for the stellar masses we also assume a 1D normal distribution, symmetrizing the $\pm 1\sigma$ error quantiles about the median.

3 Results

In Fig. 5.1 we show mass-central metallicity relation (M_*–Z_0) for our galaxies. Unsurprisingly, we recover the same positive trend that others find at lower redshift (e.g. Tremonti et al. 2004; Foster et al. 2012). However, we also observe a another dependence between the central metallicity and the metallicity gradient. It is clearly visible that at fixed mass galaxies with more positive metallicity gradients have lower central metallicities.

Our M_*–Z_0 relation appears to shows more scatter than the low redshift M_*–Z_0 relationships in the literature. However, it is important to realise that our results are not necessarily directly comparable with these. The M_*–Z_0 in the literature typically use metallicities integrated over some spatial region. For instance, the widely used SDSS results from Tremonti et al. (2004) are based on spectra of a region that contains on average 30% of the total light of the galaxy. Like other studies, Tremonti et al. (2004) make no attempt to infer the metallicity at the exact ($r = 0$) centre of a galaxy. That said, if galaxies are exponential disks and have a common metallicity gradient when expressed in scale-lengths (e.g. Sánchez et al. 2014), the central and light-weighted integrated metallicity are related by a constant factor.

Nevertheless if we take our results at face value, the scatter in the M_*–Z_0 relation is explained by the metallicity gradient. Given that low-redshift galaxies have a common metallicity gradient, one might naturally expect to see less scatter in the low-redshift M_*–Z_0 relation.

It is interesting to note that we do not observe significant trends between the central metallicity and SFR (at fixed mass). We therefore do not recover a M_*–Z_0–SFR relation that we might have expected (Lara-López et al. 2010; Mannucci et al. 2010). We will discuss the potential implications of this in Section 4.1.

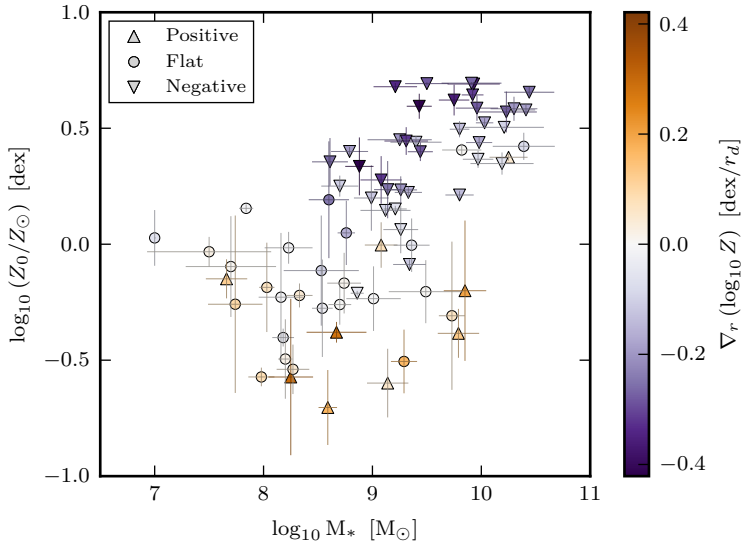

Figure 5.1: Datapoints indicate the central metallicities and metallicity gradients of our galaxy sample. The $\pm 1\sigma$ errors are drawn for each galaxy. Colours indicate the galaxy's metallicity gradient. Galaxies that have 2σ significant positive/negative gradients are labelled as up/down pointing triangles. Galaxies which have metallicity gradients that are consistent with zero (i.e. flat) are drawn as circles. Here and throughout this work solar metallicity, $Z_\odot$, equates to an oxygen abundance of $12 + \log_{10}(\mathrm{O/H}) = 8.69$ (Grevesse et al. 2010).

3.1 Analysing a M_*–Z_0–$\nabla_r (\log_{10} Z)$ relation

We wish to fit an analytical function that describes the central metallicity of a galaxy as function of its stellar mass and its metallicity gradient. In addition, although we do not observe a strong redshift dependence, we will also permit some additional dependence of the central metallicity on redshift.

As noted in the Section 2, the uncertainties in the central metallicity and the metallicity gradient are correlated. Our model fit must account for this covariance, as well as the uncertainty the stellar mass. To achieve this we will use a hierarchical Bayesian approach that we shall now outline. We present a graphical representation of the hierarchical model in Fig. 5.2.

From visual inspection of Fig. 5.1 it appears appropriate to adopt a function with a constant M_*–Z_0 slope that can be shifted vertically for different metallicity gradients. Therefore we will fit the following function for the central metallicity of the i^{th} galaxy

$$\log_{10} Z_{0,i} = \alpha + \beta\,(\log_{10} M_{*,i} - 9) + \gamma\,\nabla_r (\log_{10} Z)_i + \frac{\delta}{1+z_i}, \tag{5.1}$$

where α, β, γ and δ are the regression coefficients that we are interested in. For each galaxy: $\log_{10} M_{*,i}$ is the stellar mass, $\nabla_r (\log_{10} Z)_i$ is the metallicity gradient, and z_i is the measured redshift. The variables $\log_{10} M_{*,i}$ and $\nabla_r (\log_{10} Z)_i$ are not observed directly, in the modelling terminology these are *latent* variables and we will use this term in the following. While we do not know the true stellar mass and true metallicity gradient, we do of course have constraints on their values. The latent variables and regression coefficients are sampled from uniform priors as shown in Fig. 5.2.

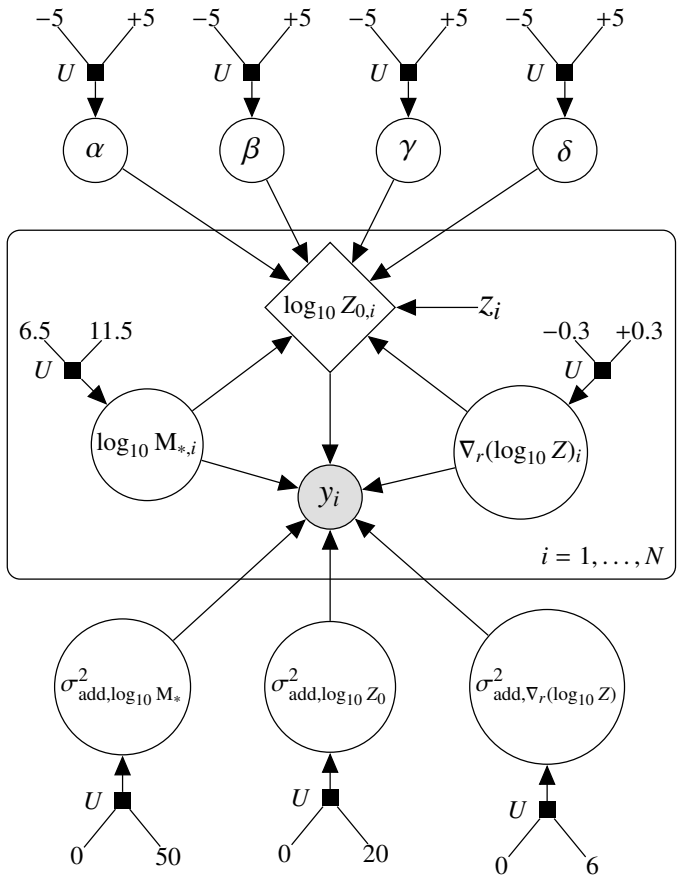

Figure 5.2: A directed factor graph representation of our hierarchical model. See text for a detailed model description. Unshaded circles represent latent (hidden) variables. The shaded circle represents the likelihood function. Diamonds indicate deterministic variables. Variables and numbers not enclosed in any shape are constants. Small black squares represent stochastic distributions. Here these distributions are all uniform, U, where their minima and maxima are indicated by their inputs.

We adopt a multinormal distribution for likelihood function of the observed mass, central metallicity and metallicity gradient

$$P\left(y_i|\log_{10}\mathrm{M}_{*,i},\log_{10}Z_{0,i},\nabla_r\left(\log_{10}Z\right)_i\right)=\mathcal{N}\left(\mu_i,\Sigma_i\right), \tag{5.2}$$

where μ_i is the mean vector

$$\mu_i=\left[\log_{10}\mathrm{M}_{*,i}\quad\log_{10}Z_{0,i}\quad\nabla_r\left(\log_{10}Z\right)_i\right], \tag{5.3}$$

and Σ_i the covariance matrix

$$\Sigma_i=\begin{bmatrix}\sigma^2_{i,\mathrm{M}_*}+\sigma^2_{\mathrm{add},\mathrm{M}_*} & 0 & 0\\ 0 & \sigma^2_{i,Z_0}+\sigma^2_{\mathrm{add},Z_0} & \mathrm{cov}_i(Z_0,\nabla_r Z)\\ 0 & \mathrm{cov}_i(Z_0,\nabla_r Z) & \sigma^2_{i,\nabla_r Z}+\sigma^2_{\mathrm{add},\nabla_r Z}\end{bmatrix}. \tag{5.4}$$

N.B. For clarity in the above matrix we have omitted the $\log_{10}$ factors from the notation. The variances, σ^2_i, and the covariances, cov_i, are given by our fitting procedure for each galaxy. Acknowledging that our model might not capture all details of the galaxies and hence that these (co-)variances might be underestimated, we allow for an additional source of uncertainty. These σ^2_{add} parameters are treated as latent variables in the model and are sampled from uniformly distributed priors over the ranges indicated in Fig. 5.2. We are not interested in these parameters and marginalise over them.

3.1.1 Fitting results

The inferred mean values of α, β, γ and δ are

$$\alpha=-0.362,\ \ \beta=0.199,\ \ \gamma=-1.57,\ \ \delta=0.455,$$

with covariances

$$\Sigma_{\alpha\beta\gamma\delta}=\begin{bmatrix}0.0335 & -0.0020 & 0.0009 & -0.0461\\ -0.0020 & 0.0012 & 0.0022 & 0.0027\\ 0.0009 & 0.0022 & 0.0265 & 0.0016\\ -0.0461 & 0.0027 & 0.0016 & 0.0651\end{bmatrix}.$$

We compare the best fit model to the data in Figs. 5.3 & 5.4, which show two different projections of the parameter space. From both figures it can be seen that the model provides a reasonable description of the data. On the vertical axes we plot the central metallicity of a galaxy, extrapolated to $z=0$. We do this to reduce the dimensionality of the data, making the plotting easier. Note that because the redshift dependence is relatively weak, and so, even though we span a modest range in redshift, the central metallicities of the galaxies are only revised by a small amount between +0.05 and +0.21 dex, depending on the galaxy's redshift.

Earlier (Section 2) we mentioned that we expect the errors of the metallicity gradient and central metallicity to be anti-correlated. Indeed we can observe the correlated errors in Fig. 5.3. However, it is worth noting that errorbars are typically much smaller than the spread of the data. Therefore there is a clearly real anti-correlation between metallicity gradient and central metallicity, i.e. beyond one that cloud have simply arisen from a degeneracy between the parameters.

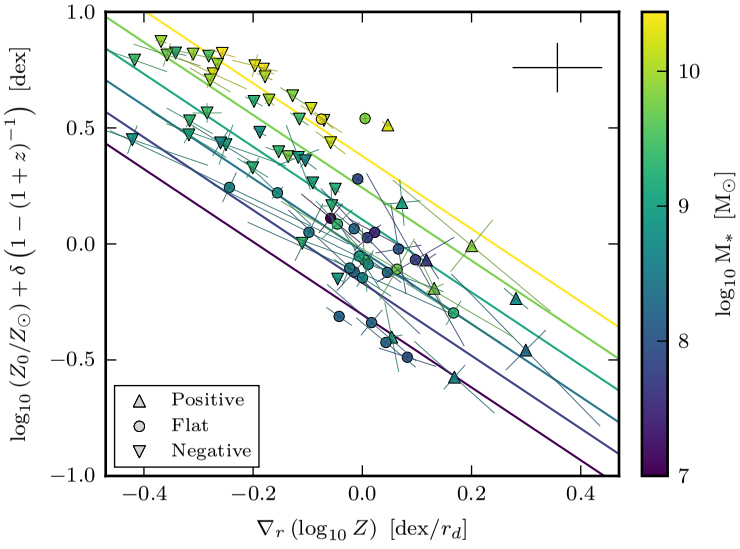

Figure 5.3: Comparison of model to data, showing metallicity gradient vs central metallicity (extrapolated to $z = 0$). The redshift dependence is taken out by the $\delta\left(1 + (1 + z)^{-1}\right)$ term, where $\delta = 0.455$ is best fit model value. The $\pm 1\sigma$ errors are drawn for each galaxy datapoint. Colours indicate the galaxy's total stellar mass. Symbol shape indicates the type of metallicity gradient: positive, flat, negative. Thick coloured lines indicate the best fit model to the data, as tracks of constant mass. The modelled additional uncertainty is plotted as a black error cross in the top-right corner of the panel.

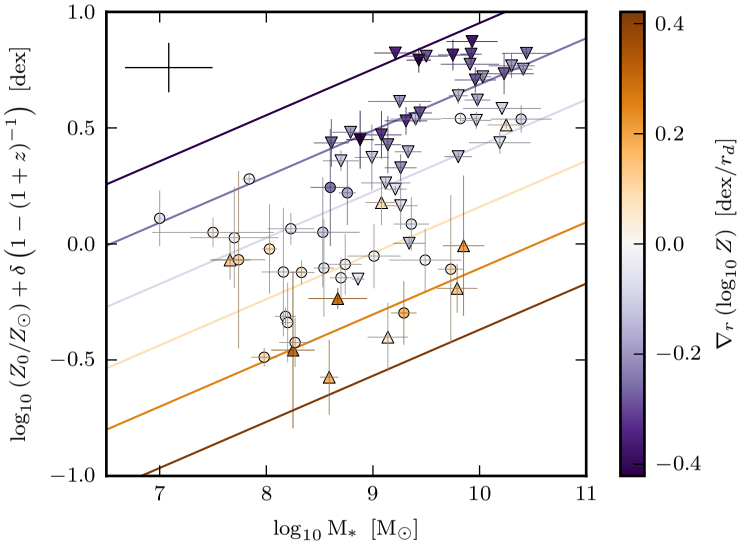

Figure 5.4: Comparison of model to data, showing stellar mass vs central metallicity (extrapolated to $z = 0$), coloured to indicate the galaxy's metallicity gradient. Thick lines indicate the best fit model to the data, as tracks of constant metallicity gradient. For a full description of the plot, see caption of Fig. 5.3.

4 Discussion

In the previous section we identified that while our galaxy sample does not present a strong M_*–Z_0 relation, this can be explained by the strong dependency between the central metallicity and the metallicity gradient.

It is not surprising that at fixed stellar mass we observe an anti-correlation between $\log_{10} Z_0$ and $\nabla_r (\log_{10} Z)$. Consider the following reasoning. Our current understanding is that galaxies grow in a self-similar inside-out fashion. And as shown by Portinari & Chiosi (1999) and Prantzos & Boissier (2000) this inside-out growth produces galaxies with negative metallicity gradients. If deviations from this (i.e. flat and positive metallicity gradients) are then caused by suppressing the central metallicity, as opposed to raising the outer metallicity, then we would expect to observe an anti-correlation between $\log_{10} Z_0$ and $\nabla_r (\log_{10} Z)$. Indeed the two common explanations of metallicity gradient inversion revolve around lowering the metallicity at the galaxy centre.

The first explanation is that the central metallicity is spuriously low because a significant amount of metal-poor gas has been deposited into the centre of the galaxy. This metal-poor gas could be acquired in a variety of ways. One mechanism invokes cold flows of metal-poor gas which originate from beyond the halo and are able to accrete directly onto the galaxy centre (Cresci et al. 2010). However, at late times ($z < 1.8$) this mechanism is less favourable because cold-flows are expected to be less common (Woods et al. 2014). So, metal-poor gas in the outskirts of a galaxy's disc could provide an alternative source. Tidal encounters with other galaxies may trigger the infall of this gas through the disc (Rupke et al. 2010; Torrey et al. 2012). That said, while galaxy–galaxy interactions can produce galaxies with flat metallicity gradients, it remains unclear whether such interactions can truly inverted metallicity gradients.

A second explanation for the metal-poor galaxy centres invokes strong centrally-concentrated winds. These winds entrain metals in the outflows, stripping metals from the gas and thereby lowering the metallicity at the centre of the galaxy. While a wind that simply blows the metal enriched gas away from the galaxy might be inefficient (Cresci et al. 2010), the accretion of this metal enriched gas onto the outskirts of the galaxies would in fact make this process rather more efficient at inverting/flattening metallicity gradients (Troncoso et al. 2014). Note that there might be some delay between the time when the central starburst occurs in a galaxy and the time when we observe it with a raised outer metallicity.

In theory, by studying both the central metallicity and the metallicity gradients of galaxies, we may be able to distinguish the inflow and outflow mechanisms. Of course, in reality the two scenarios need not be mutually exclusive, the extra gas brought by inflows may trigger intense star-formation activity that subsequently launches the centrally-concentrated outflows.

In either case (inflows or outflows), we should expect to observe elevated SFRs in galaxies with spuriously low central metallicities. However, it was a key result of our previous work that we do not see a significant correlation between the SFR and the metallicity gradient of a galaxy (Chapter 4). Similarly and although not shown here, we do not observe a significant dependence of the M_*–Z_0 relation with the total SFR. We shall discuss this further in the following section.

4.1 Implications for a M_*–Z–SFR relation

Numerous studies have demonstrated that at fixed stellar mass there is an anti-correlation between SFR and metallicity (e.g. Andrews & Martini 2013; Salim et al. 2014). Moreover some have even suggested that there exists a fundamental M_*–Z–SFR plane on which all galaxies lie, independent of redshift (Lara-López et al. 2010; Mannucci et al. 2010). Although,

because many of these studies disagree on the strength of the dependency, the universality of such a relation remains difficult to verify.

To add to this confusion, our results suggest that there is no SFR dependency at $0.1 \lesssim z \lesssim 0.8$. However, as we shall now explain, our result may not actually be in strong contradiction with these results.

At low redshift much of the M_*–Z–SFR work has been performed with multi-object fibre spectroscopy. Thus many studies observe metallicity and SFR within a small aperture at the centre of the galaxy. In contrast, we have measured the metallicity at the centre of our galaxies, but use the total SFR of the galaxy.

Had we been able to resolve a central SFR, we might have found a dependency of $\log_{10} Z_0$ on SFR, at fixed stellar mass. Similarly, although not identically, we might have found a dependency of the globally averaged metallicity on the total SFR. Although seemingly subtle, the distinction between these two points should depend on whether the chemical evolution of galaxies is regulated on local scales within galaxies, or whether it is only regulated at the global scales.

Therefore we suggest that, while we see that the central metallicity depends on metallicity gradient, it is not so surprising that we do not see a similar correlation with the SFR. Additional, indirect support for this comes from recent work of Bothwell et al. (2016) who consider dependency with a fourth quantity, the molecular gas mass, M_{H_2}. With this they identity a M_*–Z_0–M_{H_2} relation that they claim to be more fundamental than a M_*–Z_0–SFR relation. In other words, there is a more direct dependency between metallicity and molecular gas mass, than between metallicity and SFR. Combined with the above described aperture effects, this might explain our sensitivity to metallicity gradient, but not SFR.

5 Summary

We present the stellar masses, central metallicities and metallicity gradients for a sample of 72 galaxies between $0.13 < z < 0.84$. Our methodology accounts for the correlated uncertainties between the central metallicity and the metallicity gradient.

- Our key result is that, at fixed stellar mass, we find an anti-correlation between the metallicity gradient and central metallicity. This naturally would be expected if a process had recently lowered the central metallicity in the galaxies that fall below the M-Z relation.

- Given the oft-reported relation between mass, metallicity and SFR relation, we might therefore expect to see a correlation between the SFR and the metallicity gradient. However, we do not find such a correlation. We reconcile this by suggesting that because we compare the *global* SFR to a *local* metallicity measurement, we may be largely insensitive to such trends. Therefore our results do not refute the existence of a mass – metallicity – SFR relation.

We must add caution that our results are based on a relatively small sample, and since we have a sample spanning a large range of masses and SFRs (with no simple selection criteria), the strength of our conclusions are limited.

Nevertheless, our results clearly motivate further studies with current integral field spectrographs, where one can study the spatially resolved masses, SFRs and metallicities of galaxies.

Acknowledgements

JB acknowledges support from FCT grant IF/01654/2014/CP1215/CT0003.

Additionally we wish to acknowledge both the PYTHON programming language that was both used extensively throughout this work.

Bibliography

Andrews B. H., Martini P., 2013, ApJ, 765, 140
Bacon R., et al., 2010, in Ground-based and Airborne Instrumentation for Astronomy III. p. 773508, doi:10.1117/12.856027
Bothwell M. S., Maiolino R., Kennicutt R., Cresci G., Mannucci F., Marconi A., Cicone C., 2013, MNRAS, 433, 1425
Bothwell M. S., Maiolino R., Cicone C., Peng Y., Wagg J., 2016, A&A, 595, A48
Bouché N., et al., 2010, ApJ, 718, 1001
Carton D., et al., 2017, MNRAS, 468, 2140
Cresci G., Mannucci F., Maiolino R., Marconi A., Gnerucci A., Magrini L., 2010, Nature, 467, 811
Davé R., Finlator K., Oppenheimer B. D., 2012, MNRAS, 421, 98
Ellison S. L., Patton D. R., Simard L., McConnachie A. W., 2008, ApJ, 672, L107
Finlator K., Davé R., 2008, MNRAS, 385, 2181
Foster C., et al., 2012, A&A, 547, A79
Garnett D. R., 2002, ApJ, 581, 1019
Grevesse N., Asplund M., Sauval A. J., Scott P., 2010, Ap&SS, 328, 179
Kewley L. J., Dopita M. A., 2002, ApJS, 142, 35
Kriek M., van Dokkum P. G., Labbé I., Franx M., Illingworth G. D., Marchesini D., Quadri R. F., 2009, ApJ, 700, 221
Lara-López M. A., et al., 2010, A&A, 521, L53
Lequeux J., Peimbert M., Rayo J. F., Serrano A., Torres-Peimbert S., 1979, A&A, 80, 155
Lilly S. J., Carollo C. M., Pipino A., Renzini A., Peng Y., 2013, ApJ, 772, 119
Mannucci F., Cresci G., Maiolino R., Marconi A., Gnerucci A., 2010, MNRAS, 408, 2115
Portinari L., Chiosi C., 1999, A&A, 350, 827
Prantzos N., Boissier S., 2000, MNRAS, 313, 338
Rupke D. S. N., Kewley L. J., Barnes J. E., 2010, ApJ, 710, L156
Salim S., Lee J. C., Ly C., Brinchmann J., Davé R., Dickinson M., Salzer J. J., Charlot S., 2014, ApJ, 797, 126
Sánchez S. F., et al., 2014, A&A, 563, A49
Skillman E. D., Kennicutt R. C., Hodge P. W., 1989, ApJ, 347, 875
Torrey P., Cox T. J., Kewley L., Hernquist L., 2012, ApJ, 746, 108
Tremonti C. A., et al., 2004, ApJ, 613, 898
Troncoso P., et al., 2014, A&A, 563, A58
Woods R. M., Wadsley J., Couchman H. M. P., Stinson G., Shen S., 2014, MNRAS, 442, 732